THE ASTROPHYSICAL JOURNAL, 279:125–135, 1984 April 1

OPTICAL H II REGIONS IN THE OUTER GALAXY

MICHEL FICH
Radio Astronomy Laboratory, University of California, Berkeley
AND
LEO BLITZ
Astronomy Program, University of Maryland
Received 1983 June 21; accepted 1983 September 14

ABSTRACT

The distribution of optical H II regions (and their associated molecular clouds) in the outer Galaxy is found as a function of galactic radius (R) and in the direction perpendicular to the galactic plane (z). Optical distances are used where available. For the remainder of the H II regions, kinematic distances are determined using CO velocities of the associated molecular clouds and the CO rotation curve of the outer Galaxy.

In three different directions ($l \approx 95°, 150°, 210°$) a significant number of H II regions are seen at large distances, but in all cases the most distant are found near $R \approx 20$ kpc. This appears to be the limit of the radial extent of H II regions in our Galaxy. The dispersion of z distances varies between 60 and 130 pc between $R = 7$ kpc and 13 kpc and increases to ~ 300 pc at $R = 15$ kpc. There is evidence that the scale height of H II regions decreases in the spiral arms. The mean diameters of the H II regions in our sample decreases with increasing galactic radius, an effect which may be due to either a decreasing ambient gas density, a decreasing efficiency with which the highest mass stars are formed, or both.

Subject headings: galaxies: Milky Way — galaxies: structure — interstellar: molecules — nebulae: H II regions

I. INTRODUCTION

H II regions are one of the clearest tracers of star formation and galactic structure in the disks of spiral galaxies. Consequently, many attempts have been made to determine the structure of the Milky Way using galactic H II regions. Becker and Fenkart (1970) review much of the early optical work, while more recent optical work is discussed by Georgelin, Georgelin, and Sivan (1979). Mezger (1970) and Lockman (1979) have used radio recombination lines to extend this kind of study farther into the inner Galaxy. In this paper we use the results of the CO survey of optical H II regions of Blitz, Fich, and Stark (1982, hereafter BFS) to obtain the distribution of H II regions (and consequently of their associated giant molecular clouds) beyond the solar circle.

Following a discussion of the data base (§ II), and the distance determinations (§ III), the radial extent of galactic H II regions is presented in § IV*a*. This quantity allows a direct comparison with other spiral galaxies and is related to, if not identical with, the extent of the stellar disk of the Milky Way. The distribution of H II regions in the z-direction (the direction perpendicular to the plane) in the Galaxy for R (distance from the galactic center) greater than 7 kpc is given in § IV*b*. In § IV*c*, the optical angular diameters of the H II regions are used to determine the size distribution of H II regions as a function of R. A summary of the most important results is given in § V.

II. DATA

We use as a data base the catalog of CO velocities of optical H II regions of BFS. The catalog is a compilation of the radial velocities of the CO cloud complexes associated with all of the northern optical H II regions in the Galaxy which have been identified to date. The observations were made using the 5 m telescope at the Millimeter Wave Observatory in Fort Davis, Texas and the 7 m telescope at the Bell Telephone Laboratories in Crawford Hill, N.J. Details regarding the equipment and observing techniques can be found in BFS.

The use of this catalog has several advantages over other catalogs for determining the extent of star formation in the Galaxy. The uncertainties in the measured velocities of the CO complexes are ~ 1 km s^{-1} which is much smaller than the typical velocities measured. The uncertainties in the derived kinematic distances are therefore dominated almost completely by the random and systematic noncircular motions of the complexes, and by uncertainties in the determination of the rotation curve outside the solar circle. Second, the catalog is not limited by instrumental sensitivity because even the most distant H II regions have strong CO lines which are detectable in less than 1 minute. Upper limits have been found for the H II regions in which no CO was detected; the CO in those regions must have line strengths which are at least a factor of 4 smaller than the weakest line identified with any other region. Third, the catalog contains observations of 62 H II regions in addition to those in the catalog of Sharpless (1959). Many of these were previously uncatalogued. Fourth, extrapolating from observations of H II regions associated with local molecular cloud complexes, the H_2 masses are much larger than either the stellar or H II region masses (Blitz 1978) and the CO velocity should be an accurate indicator of the center-of-mass velocity of the complex. Hα and recombination line velocities, for example, tend to exhibit radial outflows with respect to the CO (see Israel 1979; Fich, Treffers, and Blitz 1982).

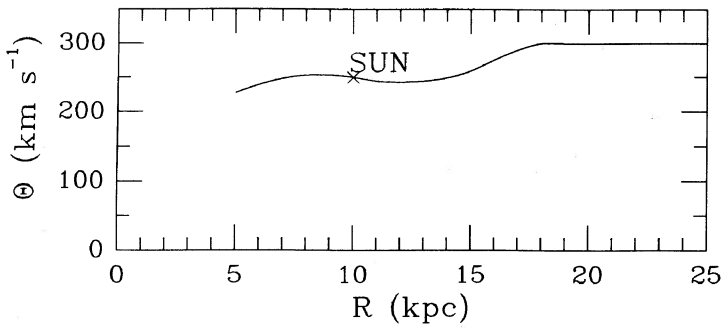

FIG. 1.—The rotation curve used to calculate kinematic distances

Therefore, as long as the assumption that the CO cloud complexes are associated with the H II regions is valid (see BFS for discussion of this point), the information in the catalog will give an accurate indication of the distribution of star-forming areas in the Galaxy. In order to verify this assumption, many of the most distant objects were mapped, and we expect that our results are not significantly affected by misidentification.

III. DISTANCES TO THE H II REGIONS

a) Method

The method of determining the kinematic distance to an object uses the radial velocity (V_r) measured for each object, the rotation curve of the Galaxy, and the assumption that all objects are in purely circular motion. The angular galactic rotation velocity ω of each object is given by:

$$\omega = \frac{V_r \cos b}{R_0 \sin (l)} + \omega_0 , \qquad (1)$$

where l and b are the galactic longitude and latitude of the object and R_0 and ω_0 are the Sun's galactocentric distance and angular galactic rotation velocity. We use $R_0 = 10$ kpc and $\omega_0 = 25$ km s^{-1} kpc^{-1}. Numerical interpolation on a rotation curve (ω vs. R) is used to calculate the value of R appropriate for each object. The composite rotation curve shown in Figure 1 is used for the interval of $R = 7$–18 kpc. This curve is based on H I terminal velocities from the first longitude quadrant of the inner Galaxy (Burton and Gordon 1978) and the CO velocities and the distances of the exciting stars of optical H II regions in the outer Galaxy (Blitz, Fich, and Stark 1980). For $R > 18$ kpc, a flat rotation curve at $\Theta = 300$ km s^{-1} ($\omega = 300/R$ km s^{-1} kpc^{-1}) is used. The location of a given H II region is obtained by determining d (the distance from the Sun to the object) and z (the distance from the mean plane) from simple geometry.

The angular diameters of the H II regions from measurements on the red Palomar Sky Survey prints were used to obtain the linear diameters of the regions.

b) Effect of Uncertainties

There are a number of uncertainties which enter into the distance determinations. For objects with optical distances, the quality of the distance determination depends on the number of stars for which spectrophotometry has been obtained. The uncertainties even for the most distant objects are, however, generally no more than 25%. For objects with kinematically determined distances, the distances are only as accurate as the rotation curve and the assumption of circular rotation which has been used to derive it. The accuracy of the outer Galaxy rotation curve has been discussed by Blitz and Fich (1983), who conclude that unless the galactic rotation constants are outside the range accepted by most observers, the rotation curve at $R > R_0$ rises in a manner similar to the one we have used. Nevertheless, we consider how the results are affected by a flat rotation curve and if the rotation constants $\Theta_0 = 220$ km s^{-1} and $R_0 = 8.5$ kpc are used.

For a flat rotation curve, the kinematic distances for objects with $R < 14$ kpc are negligibly changed. At larger distances, the galactocentric distances are reduced by about 17%. Using the smaller rotation constants decreases the distance of all the objects. However, nearby objects are affected more than the distant ones. For $R < 14$ kpc, distances are lowered by about 15%, but for objects at 20 kpc, the distances are only 2% lower.

A potentially serious error can result from noncircular motions such as the apparent ~ 10 km s^{-1} streaming motions in the Perseus arm. In the case of the Perseus arm itself, use of kinematic distances can overestimate the distances from the Sun by as much as 50%, but because of their favorable longitude and relatively small solar distances, the error in R is less than 10%. If a similar streaming motion were present in a more distant object, the error in the determination of its distances from the Sun would be smaller since the magnitude of the streaming motion would be a much smaller fraction of the measured radial motion, and once again the error in R is typically less than 10%. However, it is possible that there may be larger streaming motions in some individual objects causing significant distance errors.

Random cloud velocities of about 7 km s^{-1} (Blitz, Fich, and Stark 1980), will produce random kinematic distance uncertainties which are important for objects near the Sun but are relatively unimportant for more distant objects. These uncertainties may affect the derived size distribution of the H II regions (§ IV*c*) and are discussed in that section.

We conclude that random errors can affect the distance estimates of an individual H II region by 10%–25% whether the distances are spectrophotometrically or kinematically determined, but these uncertainties do not affect our overall results. Systematic distance errors due to uncertainties in the kinematics may cause the H II regions to have smaller galactocentric distances than those shown in Figure 2, but not by more than $\sim 15\%$ on average.

TABLE 1

POSITIONS OF H II REGIONS

Object	l	b	V_{co} (km s^{-1})	R (kpc)	d (kpc)	z (pc)	D (pc)	Comments[a]
S8	351.36	0.61	−4.3	8.32 ± 0.36	1.70 ± 0.30	18 ± 3	59.3 ± 10.5	
S11	352.80	0.64	−3.9	8.28 ± 0.36	1.74 ± 0.30	19 ± 3	45.6 ± 7.9	
S25	5.95	−1.30	12.0	8.21 ± 0.24	1.80 ± 0.20	−41 ± 5	47.1 ± 5.2	
S27	4.24	22.51	3.0	9.83 ± 0.05	0.17 ± 0.05	71 ± 21	23.7 ± 7.0	
S29	6.90	−2.45	11.0	8.71 ± 0.57	1.30 ± 0.50	−56 ± 21	15.1 ± 5.8	(S25)
S30	7.04	−0.26	...	8.22 ± 0.24	1.80 ± 0.20	−8 ± 1	10.5 ± 1.2	
S31	7.29	−2.11	8.7	9.16 ± 0.29	0.85 ± 0.27	−31 ± 10	2.0 ± 0.6	(S25)
S32	7.36	−2.09	8.9	8.22 ± 0.72	1.80 ± 0.60	−66 ± 22	4.2 ± 1.4	(S25)
S35	10.94	−1.64	...	8.43 ± 0.70	1.60 ± 0.60	−46 ± 17	9.3 ± 3.5	
S37	11.40	−1.71	12.8	9.41 ± 0.21	0.60 ± 0.20	−18 ± 6	3.5 ± 1.2	
S41	13.43	−1.40	16.8	7.88 ± 0.49	2.20 ± 0.40	−54 ± 10	57.6 ± 10.5	(S45)
S44	14.02	−0.13	19.3	7.98 ± 0.73	2.10 ± 0.60	−5 ± 1	36.7 ± 10.5	(S45)
S45	15.00	−0.68	20.0	7.90 ± 0.24	2.20 ± 0.20	−26 ± 2	38.4 ± 3.5	
S46	15.42	3.31	18.0	8.09 ± 0.83	2.00 ± 0.70	116 ± 41	14.5 ± 5.1	
S48	16.58	−0.35	44.6	7.27 ± 1.19	2.90 ± 0.90	−18 ± 6	8.4 ± 2.6	
S49	17.06	0.70	24.2	7.92 ± 0.27	2.20 ± 0.22	27 ± 3	57.6 ± 5.8	
S50	16.92	−1.07	...	8.39 ± 0.57	1.70 ± 0.50	−32 ± 9	17.3 ± 5.1	
S53	18.21	−0.32	50.0	5.78 ± 0.45	4.65 ± 1.27	−26 ± 7	20.3 ± 5.6	K
S54	18.90	2.09	27.6	8.13 ± 0.35	2.00 ± 0.20	73 ± 7	81.4 ± 8.1	
S56	21.73	−0.02	69.9	5.25 ± 0.29	5.57 ± 1.04	−2 ± 0.4	11.3 ± 2.1	
S57	22.89	0.67	(99.0)	8.64 ± 0.68	1.50 ± 0.40	18 ± 5	0.9 ± 0.2	
S58	23.13	0.54	37.2	7.24 ± 0.45	3.11 ± 0.93	29 ± 9	7.2 ± 2.2	K
S59	24.48	−0.20	45.1	6.89 ± 0.42	3.60 ± 0.98	−13 ± 3	20.9 ± 5.7	K
S60	25.36	0.24	43.8	7.05 ± 0.43	3.44 ± 0.95	14 ± 4	20.0 ± 5.5	K
S61	26.44	1.75	43.0	7.20 ± 0.39	3.30 ± 0.86	101 ± 26	1.9 ± 0.5	K
S63	27.34	−20.87	4.6	9.70 ± 0.50	0.34 ± 0.60	−129 ± 230	5.4 ± 9.6	K
S64	28.74	3.56	6.7	9.55 ± 0.47	0.52 ± 0.60	32 ± 37	3.8 ± 4.4	K
S65	29.05	−0.76	52.4	6.92 ± 0.36	3.81 ± 0.89	−51 ± 12	7.8 ± 1.8	K
S66	30.48	0.41	...	7.42 ± 1.67	3.20 ± 1.00	23 ± 7	7.4 ± 2.3	
S67	30.58	−0.73	(95.5)	9.66 ± 0.13	0.40 ± 0.10	−5 ± 1	1.2 ± 0.3	
S69	31.83	1.46	55.4	6.99 ± 0.33	3.91 ± 0.87	100 ± 22	22.7 ± 5.1	K
S70	35.13	11.36	19.8	8.93 ± 0.38	1.35 ± 0.61	271 ± 123	2.0 ± 0.9	K
S72	36.42	−1.78	64.2	6.91 ± 0.29	4.51 ± 0.95	−140 ± 29	32.8 ± 6.9	K
S73	37.62	44.71	2.4	9.92 ± 0.38	0.10 ± 0.49	100 ± 485	2.2 ± 11.0	K
S74	39.86	−1.23	48.1	7.76 ± 0.30	3.30 ± 0.80	−71 ± 17	2.9 ± 0.7	K
S77	40.56	−12.11	17.8	9.15 ± 0.33	1.16 ± 0.55	−249 ± 119	2.7 ± 1.3	K
S82	53.56	0.04	24.0	9.39 ± 0.30	1.10 ± 0.40	0.8 ± 0.3	2.9 ± 1.0	
S84	55.85	−3.80	...	8.31 ± 1.30	5.00 ± 1.60	−332 ± 106	21.8 ± 7.0	
S86	59.66	−0.21	26.8	9.19 ± 0.13	1.90 ± 0.20	−7 ± 1	22.1 ± 2.3	
S87	60.94	−0.18	22.7	9.11 ± 0.46	2.30 ± 0.70	−7 ± 2	6.7 ± 2.0	(S86)
S88	61.47	0.08	22.9	9.21 ± 0.39	2.00 ± 0.60	3 ± 1	14.5 ± 4.4	(S86)
S89	62.92	0.12	25.6	9.09 ± 0.24	2.72 ± 1.36	6 ± 3	4.0 ± 2.0	K; (S86)
S90	63.12	0.44	22.2	8.93 ± 1.05	4.00 ± 1.30	31 ± 10	7.0 ± 2.3	
S92	64.08	1.65	...	8.99 ± 1.10	4.40 ± 1.40	127 ± 40	64.0 ± 20.4	
S93	64.14	−0.47	21.3	9.24 ± 0.24	2.26 ± 1.20	−19 ± 10	0.7 ± 0.3	K; (S86)
S97	66.83	0.87	21.0	9.27 ± 0.24	2.75 ± 2.01	42 ± 31	8.0 ± 5.9	K
S99	70.15	1.71	−22.9	10.48 ± 1.47	8.00 ± 2.50	239 ± 75	11.6 ± 3.6	(S99)
S100	70.27	1.59	−24.5	10.92 ± 1.63	8.90 ± 2.90	247 ± 80	10.4 ± 3.4	
S101	71.59	2.76	13.7	9.51 ± 0.50	2.50 ± 0.80	121 ± 39	14.5 ± 4.7	
S104	74.79	0.57	0.0	9.81 ± 0.77	4.40 ± 1.40	44 ± 14	9.0 ± 2.9	
S105	75.46	2.43	...	9.77 ± 0.27	1.20 ± 0.50	51 ± 21	6.3 ± 2.6	
S106	76.40	−0.61	−1.0	10.04 ± 0.24	4.87 ± 0.98	−52 ± 8	4.2 ± 0.9	K
S107	77.39	−3.70	...	9.78 ± 0.65	2.80 ± 0.90	−181 ± 58	4.1 ± 1.3	
S108	78.18	1.80	...	9.80 ± 0.28	1.50 ± 0.40	47 ± 13	78.5 ± 20.9	
S109	79.49	0.15	...	9.84 ± 0.27	1.40 ± 0.40	4 ± 1	406.8 ± 116.2	
S112	83.78	3.28	−4.0	9.99 ± 0.42	2.10 ± 0.70	120 ± 40	9.2 ± 3.1	
S115	84.84	3.91	...	10.18 ± 0.34	3.00 ± 0.60	205 ± 41	43.6 ± 8.7	
S117	84.64	0.20	0.0	9.96 ± 0.17	0.80 ± 0.30	3 ± 1	55.9 ± 20.9	
S119	87.06	−4.19	3.5	9.99 ± 0.13	0.70 ± 0.25	−52 ± 18	32.6 ± 11.6	
S120	90.20	2.06	−65.6	13.30 ± 0.67	8.73 ± 1.02	314 ± 37	2.5 ± 0.3	K
S121	90.23	1.72	−60.9	12.90 ± 0.56	8.11 ± 0.89	244 ± 27	2.4 ± 0.3	K
S122	89.01	−41.36	−6.2	10.16 ± 0.24	1.98 ± 1.38	−1740 ± 1215	23.0 ± 16.1	K
S124	94.57	−1.45	−43.4	10.53 ± 0.16	2.60 ± 0.60	−66 ± 16	52.9 ± 12.2	
S125	94.40	−5.57	8.0	10.14 ± 0.04	1.10 ± 0.16	−107 ± 16	2.9 ± 0.4	
S126	96.72	−15.14	−0.2	10.09 ± 0.06	0.60 ± 0.20	−162 ± 54	27.9 ± 9.3	
S127	96.27	2.57	−94.7	19.39 ± 0.86	15.56 ± 1.01	698 ± 45	9.1 ± 0.6	K
S128	97.56	3.16	−72.5	14.14 ± 1.97	8.77 ± 2.76	484 ± 152	2.6 ± 0.8	K
S129	99.06	7.40	−13.9	10.07 ± 0.13	0.40 ± 0.13	52 ± 17	16.3 ± 5.3	

TABLE 1—*Continued*

Object	l	b	V_{co} (km s^{-1})	R (kpc)	d (kpc)	z (pc)	D (pc)	Comments[a]
S131	99.29	3.73	...	10.17 ± 0.10	0.86 ± 0.10	56 ± 7	42.5 ± 4.9	
S132	102.96	−0.80	−48.5	11.68 ± 1.41	4.20 ± 1.50	−59 ± 21	110.0 ± 39.3	
S134	103.72	2.18	−16.1	10.25 ± 0.33	0.90 ± 0.30	34 ± 11	41.9 ± 14.0	
S135	104.59	1.37	−20.7	10.44 ± 0.43	1.40 ± 0.40	34 ± 10	6.1 ± 1.7	
S137	105.15	7.12	−10.3	10.17 ± 0.29	0.60 ± 0.20	75 ± 25	15.7 ± 5.2	
S138	105.63	0.36	...	12.41 ± 0.49	5.13 ± 0.78	32 ± 5	4.9 ± 1.5	K
S139	105.77	−0.15	−46.5	11.35 ± 0.76	3.30 ± 1.10	−9 ± 3	24.0 ± 8.0	
S140	106.81	5.31	−8.5	10.30 ± 0.08	0.90 ± 0.10	84 ± 9	7.9 ± 0.9	
S141	106.83	3.35	−65.0	13.51 ± 0.81	6.64 ± 1.15	389 ± 67	9.7 ± 1.7	K
S142	107.28	−0.90	−41.0	11.48 ± 0.25	3.40 ± 0.30	−53 ± 5	29.7 ± 2.6	
S143	107.29	−1.43	...	11.65 ± 0.99	3.70 ± 1.20	−92 ± 30	4.3 ± 1.4	
S145	108.18	5.55	−8.8	10.32 ± 0.26	0.91 ± 0.65	88 ± 64	23.8 ± 17.1	K
S146	108.20	0.58	−49.5	12.29 ± 0.48	4.67 ± 0.76	47 ± 8	2.7 ± 0.4	K
S147	108.28	−1.08	−57.0	12.84 ± 0.60	5.51 ± 0.89	−104 ± 17	3.2 ± 0.5	K
S148	108.34	−1.05	−53.1	12.84 ± 1.21	5.50 ± 1.80	−101 ± 33	3.2 ± 1.0	(S147)
S149	108.34	−1.12	−53.1	12.77 ± 1.15	5.40 ± 1.70	−106 ± 33	1.6 ± 0.5	(S147)
S150	109.00	6.29	−8.8	10.32 ± 0.26	0.88 ± 0.64	97 ± 70	10.2 ± 7.4	K
S151	108.69	−2.63	−56.2	12.78 ± 0.56	5.37 ± 0.84	−247 ± 39	31.3 ± 4.9	K
S152	108.75	−0.93	−50.4	11.67 ± 0.81	3.60 ± 1.10	−58 ± 18	2.1 ± 0.6	
S153	108.77	−0.99	−50.6	11.91 ± 0.94	4.00 ± 1.30	−69 ± 23	5.8 ± 1.9	(S152)
S154	109.17	1.47	−11.5	10.54 ± 0.33	1.40 ± 0.40	36 ± 10	24.4 ± 7.0	
S155	110.22	2.55	−10.0	10.28 ± 0.10	0.73 ± 0.12	33 ± 5	12.7 ± 2.1	
S156	110.11	0.05	−51.0	13.60 ± 1.30	6.40 ± 2.00	6 ± 2	3.7 ± 1.2	
S157	111.28	−0.66	−43.0	11.15 ± 0.32	2.50 ± 0.40	−29 ± 5	65.4 ± 10.5	
S158	111.54	0.78	−56.1	11.33 ± 0.35	2.80 ± 0.90	38 ± 12	8.1 ± 2.6	
S159	111.61	0.37	−56.0	12.85 ± 0.60	5.19 ± 0.87	34 ± 13	10.6 ± 1.8	K
S160	111.93	4.08	...	10.37 ± 0.26	0.90 ± 0.30	64 ± 21	20.9 ± 7.0	
S161B	111.89	0.88	−51.9	11.35 ± 0.71	2.80 ± 0.90	43 ± 14	44.8 ± 14.4	
S162	112.19	0.22	−44.7	11.78 ± 0.84	3.50 ± 1.10	13 ± 4	40.7 ± 12.8	
S163	113.52	−0.57	−44.9	11.12 ± 0.58	2.30 ± 0.70	−23 ± 7	6.7 ± 2.0	
S164	113.91	−1.62	...	12.87 ± 1.15	5.00 ± 1.60	−141 ± 45	4.4 ± 1.4	
S165	114.65	0.14	−33.0	10.77 ± 0.43	1.60 ± 0.50	4 ± 1	4.7 ± 1.5	
S167	114.99	3.21	−63.6	13.76 ± 1.28	6.13 ± 1.69	344 ± 95	3.6 ± 1.0	K
S168	115.79	−1.65	−40.6	12.15 ± 1.04	3.80 ± 1.20	−110 ± 35	7.7 ± 2.4	
S169	115.83	−1.70	−39.0	11.76 ± 0.44	3.21 ± 0.68	−95 ± 20	4.7 ± 1.0	K; (S168)
S170	117.57	2.26	−43.7	11.25 ± 0.49	2.30 ± 0.70	91 ± 28	13.4 ± 4.1	
S171	118.40	4.70	...	10.43 ± 0.08	0.84 ± 0.10	69 ± 8	44.0 ± 5.2	
S172	118.63	−1.32	−40.8	11.95 ± 0.47	3.32 ± 0.69	−77 ± 16	1.0 ± 0.2	K
S173	119.40	−0.84	−34.5	11.57 ± 0.64	2.70 ± 0.90	−40 ± 13	23.6 ± 7.9	
S174	120.17	18.40	−2.7	10.11 ± 0.27	0.22 ± 0.52	72 ± 173	0.6 ± 1.5	K
S175	120.36	1.97	−49.6	10.96 ± 0.24	1.70 ± 0.50	59 ± 17	1.0 ± 0.3	
S177	120.63	−0.14	−34.2	11.48 ± 0.37	2.50 ± 0.80	−6 ± 2	1.5 ± 0.5	
S178	125.05	25.63	−3.6	10.14 ± 0.29	0.24 ± 0.49	115 ± 236	29.4 ± 60.0	K
S181	122.72	2.37	−36.6	11.77 ± 0.47	2.83 ± 0.66	117 ± 28	12.3 ± 2.9	K
S182	122.81	1.87	−27.0	11.20 ± 0.38	1.98 ± 0.58	65 ± 19	1.2 ± 0.3	K
S183	123.00	3.02	−10.3	10.42 ± 0.30	0.74 ± 0.51	39 ± 27	7.5 ± 5.1	K
S184	123.21	−6.32	−30.4	11.35 ± 0.38	2.20 ± 0.70	−244 ± 78	25.6 ± 8.1	
S185	123.84	−1.96	−16.2	10.12 ± 0.04	0.21 ± 0.07	−7 ± 2	7.3 ± 2.4	
S186	124.89	0.32	−43.0	12.31 ± 0.59	3.46 ± 0.79	19 ± 6	1.0 ± 0.2	K
S187	126.72	−0.73	−14.9	10.65 ± 0.32	1.03 ± 0.49	−13 ± 6	3.0 ± 1.4	K
S190	133.71	1.21	−46.0	11.55 ± 0.14	2.10 ± 0.20	44 ± 4	91.6 ± 8.7	
S192	136.13	2.08	−46.3	13.41 ± 1.14	4.27 ± 1.34	155 ± 49	1.2 ± 0.4	K
S193	136.09	2.12	−47.2	13.54 ± 1.84	4.42 ± 2.14	164 ± 79	2.6 ± 1.2	K; (S192)
S194	136.14	2.07	−46.5	13.44 ± 1.20	4.31 ± 1.39	156 ± 50	2.5 ± 0.8	K; (S192)
S196	136.51	2.50	−45.1	13.29 ± 1.05	4.11 ± 1.23	180 ± 54	4.8 ± 1.4	K
S198	137.38	0.20	...	12.29 ± 0.84	2.90 ± 0.90	10 ± 3	7.6 ± 2.4	
S199	137.30	1.56	−39.0	11.63 ± 0.20	2.10 ± 0.20	57 ± 5	73.3 ± 7.0	
S200	138.16	4.09	−9.7	10.50 ± 0.38	0.66 ± 0.49	47 ± 35	1.1 ± 0.8	K
S201	138.47	1.60	−40.0	12.86 ± 0.88	3.53 ± 1.02	99 ± 29	5.1 ± 1.5	K
S202	139.99	2.09	−11.5	10.63 ± 0.32	0.80 ± 0.30	29 ± 11	39.6 ± 14.8	
S205	148.84	−1.24	−25.8	10.78 ± 0.34	0.90 ± 0.30	−20 ± 7	31.4 ± 10.5	
S206	150.68	−0.77	−22.6	12.98 ± 0.76	3.30 ± 0.80	−44 ± 11	48.0 ± 11.6	
S208	151.27	1.97	−30.2	17.06 ± 0.58	7.60 ± 0.80	261 ± 28	2.2 ± 0.2	
S209	151.61	−0.24	−52.2	21.41 ± 2.40	12.08 ± 2.47	−51 ± 10	49.2 ± 10.0	K
S211	154.65	2.46	−37.6	18.54 ± 3.35	9.00 ± 3.44	387 ± 148	5.2 ± 2.0	K
S212	155.39	2.65	−35.3	15.66 ± 0.69	6.00 ± 0.60	278 ± 28	8.7 ± 0.9	
S213	157.08	−3.61	−31.0	17.02 ± 3.37	7.36 ± 3.46	−464 ± 218	2.1 ± 1.0	K
S217	159.15	3.27	−20.5	14.98 ± 0.89	5.20 ± 0.80	297 ± 46	13.6 ± 2.1	
S218	159.61	11.36	3.4	...	...	...	...	

TABLE 1—*Continued*

Object	l	b	V_{co} (km s^{-1})	R (kpc)	d (kpc)	z (pc)	D (pc)	Comments[a]
S219	159.36	2.57	−24.5	14.01 ± 0.39	4.20 ± 0.60	189 ± 27	3.7 ± 0.5	
S220	160.61	−17.80	7.0	10.38 ± 0.04	0.40 ± 0.04	−128 ± 13	37.2 ± 3.7	
S225	168.09	3.07	...	13.64 ± 0.62	3.70 ± 0.90	198 ± 48	10.8 ± 2.6	
S227	168.70	1.00	...	14.24 ± 0.93	4.30 ± 1.40	75 ± 24	25.0 ± 8.1	
S229	171.35	−2.26	6.7	10.50 ± 0.15	0.51 ± 0.16	−20 ± 6	9.6 ± 3.0	
S231	173.47	2.55	−18.1	12.29 ± 0.55	2.30 ± 0.70	102 ± 31	8.0 ± 2.4	
S232	173.43	3.17	−23.0	10.99 ± 0.26	1.00 ± 0.30	55 ± 17	11.6 ± 3.5	
S234	173.48	−0.05	−13.4	12.29 ± 0.55	2.30 ± 0.70	−2 ± 1	8.0 ± 2.4	
S235	173.62	2.81	−18.8	11.59 ± 0.41	1.60 ± 0.50	79 ± 25	4.7 ± 1.5	(S231)
S236	173.60	−1.78	−7.2	13.19 ± 0.22	3.20 ± 0.30	−99 ± 9	51.2 ± 4.8	
S237	173.97	0.25	−4.3	11.79 ± 0.24	1.80 ± 0.30	8 ± 1	3.7 ± 0.6	
S238	176.24	−20.88	8.1	10.15 ± 0.05	0.15 ± 0.05	−57 ± 19	0.04 ± 0.01	
S239	178.91	−20.12	7.0	10.15 ± 0.05	0.15 ± 0.05	−55 ± 18	0.2 ± 0.05	(S238)
S241	180.79	4.03	−6.5	14.70 ± 0.79	4.70 ± 1.20	331 ± 85	13.7 ± 3.5	
S242	182.36	0.19	0.0	12.10 ± 0.56	2.10 ± 0.70	7 ± 2	4.3 ± 1.4	
S245	186.34	−34.31	...	10.21 ± 0.02	0.21 ± 0.02	−143 ± 14	44.0 ± 4.2	
S247	188.96	0.85	2.9	13.47 ± 0.64	3.50 ± 0.90	52 ± 13	9.2 ± 2.4	
S249	189.45	4.38	−5.3	11.58 ± 0.41	1.60 ± 0.50	123 ± 38	37.2 ± 11.6	
S252	189.81	0.33	7.5	11.48 ± 0.12	1.50 ± 0.15	9 ± 1	17.5 ± 1.7	
S253	192.23	3.59	14.4	14.33 ± 0.26	4.40 ± 0.40	276 ± 25	6.4 ± 0.6	
S254	192.61	−0.04	7.5	12.45 ± 0.30	2.50 ± 0.40	−2 ± 0.3	8.0 ± 1.3	
S255	192.61	−0.04	7.5	12.45 ± 0.30	2.50 ± 0.40	−2 ± 0.3	2.2 ± 0.3	(S254)
S256	192.61	−0.04	7.5	12.45 ± 0.30	2.50 ± 0.40	−2 ± 0.3	0.7 ± 0.1	(S254)
S257	192.61	−0.04	7.5	12.45 ± 0.30	2.50 ± 0.40	−2 ± 0.3	2.2 ± 0.3	(S254)
S258	192.61	−0.04	8.0	12.45 ± 0.30	2.50 ± 0.40	−2 ± 0.3	0.7 ± 0.1	(S254)
S259	192.91	−0.63	22.8	18.19 ± 1.35	8.30 ± 2.60	−91 ± 29	4.8 ± 1.5	
S263	194.59	−15.74	0.3	10.44 ± 0.13	0.45 ± 0.14	−127 ± 40	2.9 ± 0.9	
S264	196.92	−10.37	12.0	10.38 ± 0.12	0.40 ± 0.13	−73 ± 24	45.5 ± 14.7	
S265	195.23	−16.98	−1.6	...	...	...	...	
S266	195.65	−0.07	31.2	22.34 ± 3.14	12.55 ± 3.16	−15 ± 4	3.6 ± 0.9	K
S268	195.97	−2.74	4.8	10.61 ± 1.00	0.63 ± 1.04	−30 ± 50	11.0 ± 18.1	K
S269	196.45	−1.68	17.5	13.69 ± 0.75	3.80 ± 1.00	−112 ± 29	4.4 ± 1.2	
S270	196.83	−3.11	25.6	18.60 ± 4.33	8.80 ± 4.38	−478 ± 238	2.6 ± 1.3	K
S271	197.80	−2.33	20.5	14.65 ± 0.63	4.80 ± 0.50	−195 ± 20	2.8 ± 0.3	
S272	197.82	−2.33	20.6	14.64 ± 0.63	4.80 ± 0.50	−195 ± 20	1.4 ± 0.1	K; (S271)
S273	203.24	2.09	7.0	10.74 ± 0.25	0.80 ± 0.15	29 ± 6	58.2 ± 10.2	
S275	207.02	−1.82	14.3	11.45 ± 0.31	1.60 ± 0.20	−51 ± 6	46.5 ± 5.8	
S277	206.63	−16.22	9.6	10.45 ± 0.08	0.50 ± 0.05	−146 ± 15	17.5 ± 1.7	(S281)
S278	207.57	−23.07	9.2	10.45 ± 0.08	0.50 ± 0.05	−213 ± 21	7.3 ± 0.7	(S281)
S279	208.45	−19.09	8.0	10.44 ± 0.08	0.50 ± 0.05	−173 ± 17	2.9 ± 0.3	(S281)
S280	208.71	−2.64	...	11.52 ± 0.76	1.70 ± 0.50	−78 ± 23	19.8 ± 5.8	
S281	208.99	−19.39	8.0	10.44 ± 0.08	0.50 ± 0.05	−176 ± 18	8.7 ± 0.9	
S282	209.91	−2.15	23.3	11.33 ± 0.77	1.50 ± 0.50	−56 ± 19	15.3 ± 5.1	
S283	210.81	−2.56	49.4	18.42 ± 2.74	9.10 ± 2.90	−407 ± 130	7.9 ± 2.5	
S284	211.86	−1.18	45.0	14.68 ± 0.94	5.20 ± 0.80	−107 ± 17	121.0 ± 18.6	
S285	213.81	0.61	45.3	16.19 ± 0.74	6.90 ± 0.70	74 ± 8	2.0 ± 0.2	
S286	217.31	−1.39	49.8	17.79 ± 2.74	8.77 ± 2.91	−213 ± 71	15.3 ± 5.1	K
S287	218.15	−0.35	27.2	12.67 ± 1.05	3.20 ± 0.80	−20 ± 5	11.2 ± 2.8	
S288	218.77	1.95	56.7	12.48 ± 1.59	3.00 ± 1.20	102 ± 41	0.9 ± 0.3	
S289	218.85	−4.55	...	16.91 ± 0.78	7.90 ± 0.80	−629 ± 64	25.3 ± 2.6	
S292	224.10	−1.96	18.4	10.86 ± 0.21	1.15 ± 0.14	−39 ± 5	7.0 ± 0.9	
S293	224.17	−2.87	14.6	10.85 ± 0.21	1.15 ± 0.14	−58 ± 7	3.7 ± 0.4	(S292)
S294	224.19	1.22	32.9	13.68 ± 1.75	4.60 ± 1.50	98 ± 32	9.4 ± 3.1	
S295	224.41	−2.74	13.8	10.85 ± 0.28	1.15 ± 0.19	−55 ± 9	2.7 ± 0.4	(S292)
S296	224.43	−0.78	15.0	10.85 ± 0.21	1.15 ± 0.14	−16 ± 2	66.9 ± 8.1	(S292)
S297	225.44	−2.63	11.7	10.84 ± 0.20	1.15 ± 0.14	−53 ± 6	2.3 ± 0.3	(S292)
S298	227.78	−0.06	39.0	14.98 ± 2.59	6.30 ± 2.50	−7 ± 3	40.3 ± 16.0	
S299	230.97	1.49	47.6	13.22 ± 0.68	4.40 ± 0.60	114 ± 16	1.3 ± 0.2	
S300	231.01	1.55	52.8	13.22 ± 0.68	4.40 ± 0.60	119 ± 16	3.8 ± 0.5	(S299)
S301	231.52	−4.33	53.0	14.35 ± 0.94	5.80 ± 0.90	−439 ± 68	15.2 ± 2.4	
S302	232.63	1.01	16.6	11.47 ± 0.91	2.20 ± 0.70	39 ± 12	13.4 ± 4.3	
S305	233.77	−0.15	44.1	13.73 ± 1.50	5.20 ± 1.40	−14 ± 4	6.1 ± 1.6	
S306	234.28	−0.43	44.1	12.91 ± 0.45	4.20 ± 0.40	−32 ± 3	36.7 ± 3.5	
S307	234.57	0.83	46.3	11.42 ± 0.64	2.20 ± 0.50	32 ± 7	3.8 ± 0.9	
S308	234.76	−10.10	...	11.00 ± 0.92	1.60 ± 0.70	−285 ± 125	16.3 ± 7.1	
S309	234.64	−0.21	44.0	13.93 ± 0.84	5.50 ± 0.80	−20 ± 3	19.2 ± 2.8	
S310	239.65	−4.94	22.3	10.84 ± 0.64	1.50 ± 0.50	−130 ± 43	209.4 ± 69.8	
S311	243.2	0.44	51.0	12.40 ± 0.64	4.10 ± 0.60	32 ± 5	53.7 ± 7.9	
2	66.98	−1.26	11.6	9.59 ± 0.24	1.22 ± 0.93	−27 ± 21	1.8 ± 1.4	K

TABLE 1—*Continued*

Object	l	b	V_{co} (km s^{-1})	R (kpc)	d (kpc)	z (pc)	D (pc)	Comments[a]
4	90.40	2.44	1.1	...	...	...	...	*
6	95.65	0.24	−74.2	14.38 ± 2.10	9.40 ± 2.90	39 ± 12	8.2 ± 2.5	K
9	97.39	8.50	3.3	...	...	...	...	*
10	101.46	2.66	−61.0	13.01 ± 0.60	6.57 ± 0.91	305 ± 42	1.9 ± 0.3	K
11	105.38	9.88	−10.1	10.36 ± 0.25	1.14 ± 0.68	198 ± 119	3.3 ± 2.0	K
12	108.03	−0.18	−49.9	12.31 ± 0.47	4.72 ± 0.75	−15 ± 2	16.5 ± 2.3	K
14	109.05	−0.33	−47.0	12.14 ± 0.46	4.35 ± 0.73	−25 ± 5	88.7 ± 14.9	K
15	109.99	−0.08	−51.5	12.46 ± 0.51	4.76 ± 0.78	−7 ± 1	1.4 ± 0.2	K
16	110.03	0.29	−51.9	12.49 ± 0.51	4.80 ± 0.78	24 ± 4	2.8 ± 0.5	K
17	110.20	0.21	−50.8	12.42 ± 0.50	4.68 ± 0.76	17 ± 3	1.4 ± 0.2	K
18	110.24	0.16	−52.8	12.56 ± 0.52	4.89 ± 0.79	14 ± 2	1.4 ± 0.2	K
24	134.32	3.72	−9.7	10.47 ± 0.35	0.66 ± 0.48	43 ± 31	3.8 ± 2.8	K
28	141.73	2.76	−10.2	10.57 ± 0.41	0.71 ± 0.51	34 ± 24	4.2 ± 2.9	K
29	142.27	1.92	−10.9	10.62 ± 0.42	0.77 ± 0.52	26 ± 17	6.7 ± 4.5	K
31	143.81	−1.51	−32.2	12.44 ± 0.83	2.88 ± 0.94	−76 ± 25	1.7 ± 0.5	K
32	149.09	−1.98	−7.9	10.53 ± 0.50	0.61 ± 0.57	−21 ± 20	0.4 ± 0.3	K
33	150.06	−1.12	−5.5	10.38 ± 0.49	0.44 ± 0.56	−9 ± 11	0.3 ± 0.3	K
34	150.99	−0.47	−27.7	12.62 ± 1.10	2.91 ± 1.20	−24 ± 10	4.2 ± 1.7	K
35	155.53	−8.89	−7.6	10.63 ± 0.64	0.69 ± 0.70	−108 ± 110	0.6 ± 0.6	K
36	155.63	−8.68	−7.2	10.60 ± 0.64	0.65 ± 0.69	−100 ± 106	0.6 ± 0.6	K; (35)
37	156.28	−8.45	−7.5	10.64 ± 0.67	0.70 ± 0.72	−103 ± 108	0.6 ± 0.6	K
38	156.35	−8.39	−7.3	10.63 ± 0.66	0.68 ± 0.72	−101 ± 106	0.6 ± 0.6	K; (37)
39	156.42	−8.18	−5.9	10.50 ± 0.64	0.54 ± 0.70	−78 ± 100	0.5 ± 0.6	K; (37)
41	156.51	−8.24	−6.8	10.59 ± 0.66	0.64 ± 0.71	−93 ± 103	0.6 ± 0.6	K; (37)
44	160.27	0.85	−25.2	14.39 ± 3.51	4.58 ± 3.61	68 ± 54	6.7 ± 5.3	K
53	211.16	−0.99	37.1	13.96 ± 2.78	4.41 ± 3.00	−76 ± 52	2.6 ± 1.7	K
54	211.27	−0.35	21.4	18.01 ± 2.01	8.70 ± 2.80	−53 ± 17	7.6 ± 2.4	
55	216.17	−0.02	23.5	11.58 ± 0.63	1.89 ± 0.73	−1 ± 0.3	13.7 ± 5.3	K
56	217.31	−0.05	26.7	11.81 ± 0.66	2.18 ± 0.76	−2 ± 1	0.6 ± 0.2	K
57	217.39	−0.08	25.9	11.73 ± 0.63	2.09 ± 0.74	−3 ± 1	0.6 ± 0.2	K; (56)
58	217.46	0.38	49.9	17.77 ± 2.69	8.76 ± 2.86	58 ± 19	7.6 ± 2.5	K
59	216.67	−0.19	25.7	11.70 ± 0.63	2.06 ± 0.73	−7 ± 2	1.8 ± 0.6	K; (56?)
60	219.58	−3.81	11.2	10.61 ± 0.40	0.78 ± 0.51	−52 ± 34	0.2 ± 0.1	K
61	220.74	−2.17	9.9	10.52 ± 0.39	0.67 ± 0.50	−26 ± 19	0.2 ± 0.1	K
62	220.78	−1.75	13.4	10.72 ± 0.41	0.93 ± 0.52	−28 ± 16	0.5 ± 0.3	K
63	220.91	−2.48	13.4	10.72 ± 0.41	0.93 ± 0.52	−40 ± 22	2.7 ± 1.5	K
64	221.84	−2.05	40.0	12.83 ± 0.84	3.51 ± 0.98	−126 ± 35	5.1 ± 1.4	K

NOTES ON INDIVIDUAL OBJECTS.—S57: Velocity is not compatible with distance. Optical distance used. S122: Object is far from the galactic plane. Velocity is probably not representative of galactic rotation. S218: Object at "forbidden" velocity (see text). S265: Object at "forbidden" velocity. 2: Object at "forbidden" velocity. 9: Object at "forbidden" velocity.

[a] Name in parentheses is associated H II region; K means kinematic distance used.

IV. RESULTS

a) The Radial Distribution

Table 1 contains a summary of all of the data and of the calculated values of R, d (the distance from the object to the Sun), z, and D (the linear diameter) for each of the 205 optically identified objects from which CO has been detected. One hundred and six of the objects in the catalog of BFS have been excluded from this table since their radial velocities are unknown and there are no direct measurements of their distances. The column labeled "Comments" shows which objects have kinematic distances (K) calculated to them.

The uncertainties indicated in Table 1 for objects with spectrophotometric distances reflect the uncertainties in the distances as given in the catalog of BFS and references there. For those objects with kinematic distance determinations, the uncertainties are computed from the velocities assuming a random component of 7 km s^{-1} plus the uncertainty in the measured CO velocity as indicated in BFS.

The distribution of the H II regions projected onto the galactic plane is shown in Figure 2. Only kinematically distinct objects are plotted; that is, when several H II regions are part of a larger complex, only one of them is plotted so as to represent the position of the whole complex. Objects with positions determined from spectroscopic parallaxes are indicated by squares, while those with kinematic positions are indicated by crosses. Because of confusion due to the large number of objects near the Sun, this figure has been split into two parts: Figure 2*a*, containing the large-scale distribution, and Figure 2*b* which shows the objects within 1 kpc of the Sun.

Most of the H II regions seen in the general direction of the galactic center are within three kpc of the Sun since the extinction in the inner Galaxy is too large to permit optical detection of more distant objects. In the outer Galaxy, there are three "fingers" which contain objects which are as much as 15 kpc from the Sun. These fingers are due to holes in the foreground extinction and occur near $l = 95°$, $l = 150°$, and $l = 210°$. In the third quadrant ($l = 180°$–$270°$), the H II regions are more evenly distributed throughout the plane than in the rest of the area surveyed. That they are visible almost everywhere in that quadrant is indicative of the generally lower amount of extinc-

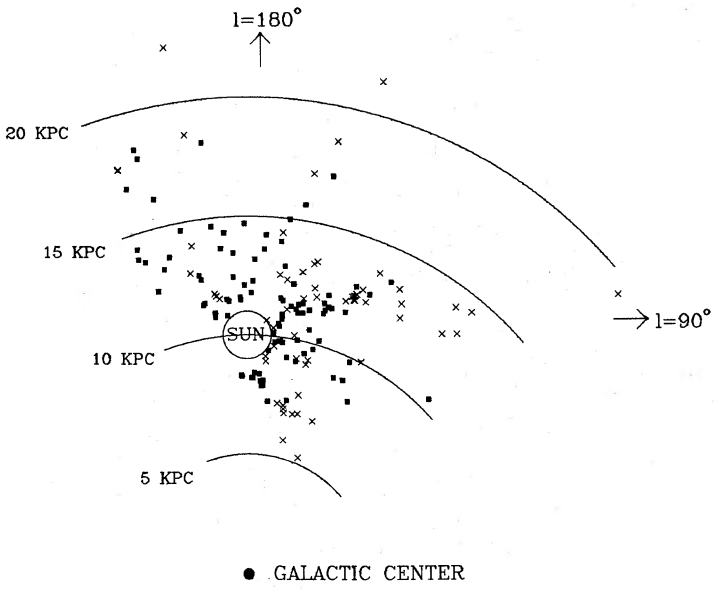

FIG. 2a

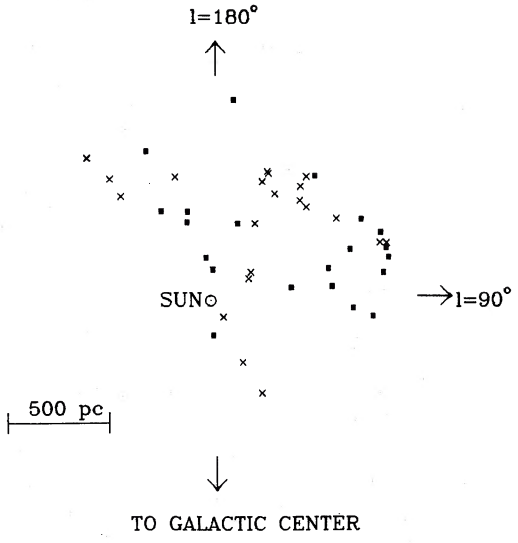

FIG. 2b

FIG. 2.—Positions of H II regions projected onto the Galactic plane. Optical positions are indicated by squares; kinematic positions by crosses. Fig. 2*a*: points within ≈1 kpc of the Sun excluded. Fig. 2*b*: small-scale view showing objects near the Sun.

tion in that part of the Galaxy. The most distant (S266) is about 22 kpc from the galactic center and about 13 kpc from the Sun. The blank area in the lower left ($l > 250°$) is too far south to be observed by the instruments used in this project. *None of the optically identified* H II *regions lie at galactocentric distances significantly larger than about 20 kpc.*

In order to determine whether the inability to detect H II regions beyond $R \approx 20$ kpc is due to extinction, we examine the run of the extinction along two of the "fingers" at $l = 150°$ and $l = 210°$. The results are shown in Figure 3 which are taken from the data of Moffat, FitzGerald, and Jackson (1979). These data indicate that the extinction along the line of sight (which includes the internal extinction of the source) is roughly constant at 3 magnitudes in much of the outer Galaxy, independent of the distance to the object. Thus, there does not appear to be a progressively rising extinction more than several kpc from the Sun to bias our results. (Similarly in M31 Kumar 1979 has found that the reddening to H II regions is substantially less for regions at $R > 12$ kpc than for those inside that distance.) Furthermore, if extinction were the sole cause of our inability to detect very distant H II regions and these objects were similar to those found locally, they would appear as bright sources in radio continuum surveys of the second and third quadrants. However, based on existing surveys, there appear to be less than 10 radio H II regions brighter than 1 Jy in those quadrants which are not associated with optical objects. A more sensitive search for such objects at 5 GHz is currently underway by Fich (1983).

H II regions appreciably smaller than 1′ are often difficult to pick out on Palomar Sky Survey plates even though the

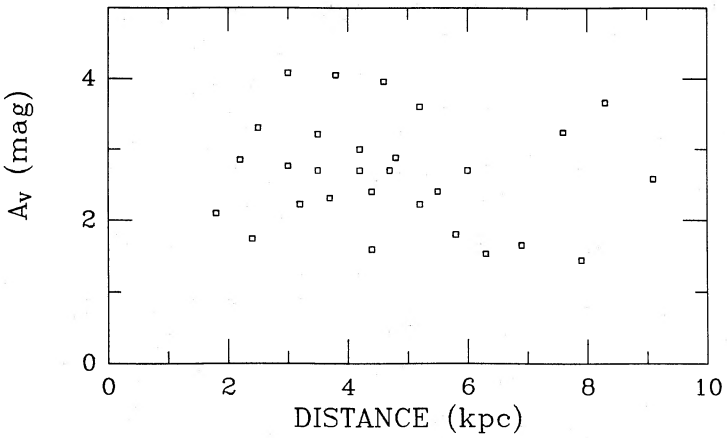

FIG. 3.—Extinction along lines of sight from the Sun between $l = 150°$ and $l = 210°$

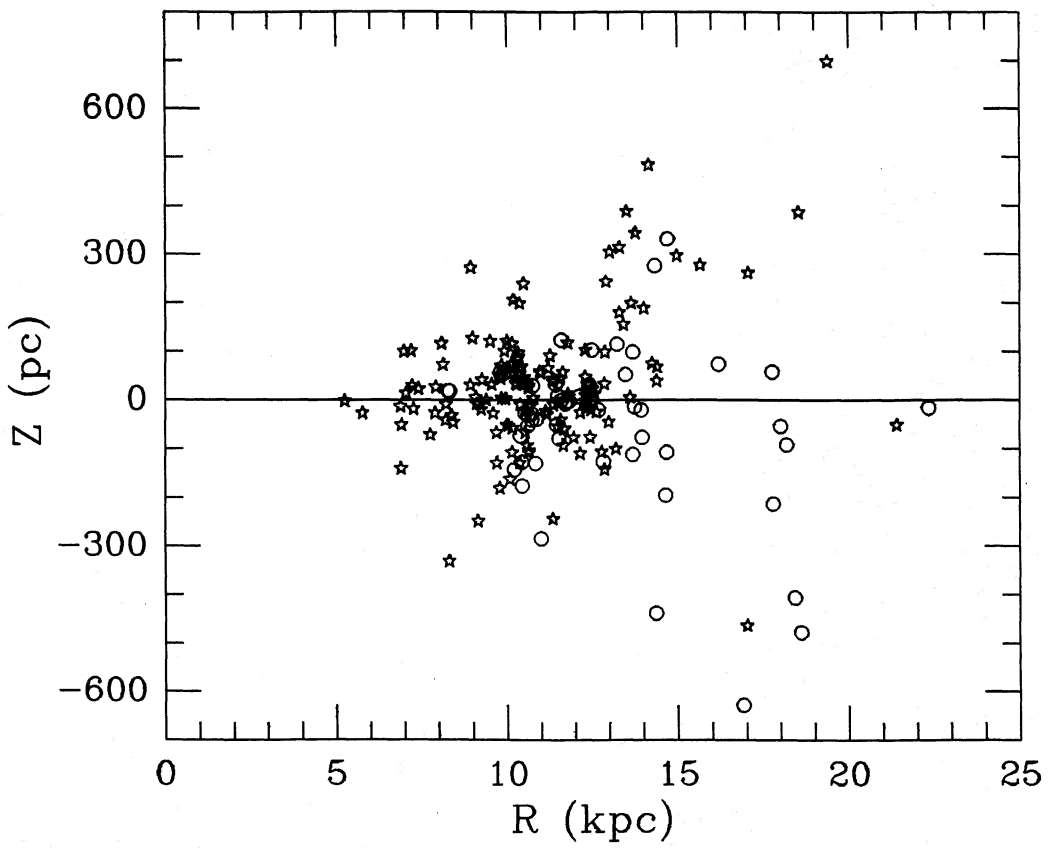

FIG. 4.—The distance above or below the plane of the Galaxy (the z distance) plotted against the distance from the center of the Galaxy (R). Northern objects are labeled with stars; southern objects are labeled with circles.

surface brightnesses of the H II regions in this sample are quite high. If H II regions do get smaller at larger R as suggested in § IV*c* or if they get less bright at larger R, we might not see them at such large distances. However, from the ease of identifying even the most distant of the H II regions on the Palomar prints (note especially that S127 is readily identifiable even though it is almost 16 kpc from the Sun), it should be possible to identify other similar H II regions, except perhaps those less than ~ 2 pc in diameter beyond $R = 20$ kpc if such existed.

The evidence therefore suggests that there is not an appreciable number of H II regions at $R \geq 20$ kpc, and massive star formation essentially ceases at that distance. If this is the case, it is possible that this distance also corresponds to the edge of the stellar disk in the Milky Way, a distance which also corresponds to a sharp decrease in the H I surface density (Blitz, Fich, and Kulkarni 1983).

b) The Distribution Perpendicular to the Plane

In Figure 4 we show the distribution of H II regions perpendicular to the plane of the Galaxy with their heights (z) plotted against their galactocentric distances. Objects between $0° < l \leq 180°$ ("northern" objects) are labeled with stars while those between $180° < l \leq 360°$ ("southern") are labeled with circles. Table 2 gives the z distribution averaged over 1 kpc intervals in R. The dispersion in the z distance of the H II regions within 12 kpc of the galactic center varies from 60 to 130 kpc. At larger distances, the dispersion of H II regions increases steadily; at $R > 14.5$ kpc it reaches about 300 pc. As a check, the dispersion was also calculated for only those objects which have optically determined distances; there were no significant differences in the results.

There is a clear difference between northern and southern objects at galactocentric distances greater than 14.5 kpc. Northern objects are found preferentially above the plane, while the southern objects are found preferentially below. This segregation between northern and southern objects follows the well-known warping of the H I plane in the outer parts of the Galaxy. We apply a correction to the scale height by determining the mean H I plane at the same velocity as the H II region (from Kulkarni, Blitz, and Heiles 1982). The result of this correction is shown in the last line of Table 2. Since the H I velocity information is not useful for two of the objects (they are in the Galactic anticenter), there are two fewer objects in the corrected z distribution in the last line of Table 2.

Another feature of the z distribution is a narrowing of the dispersion at $R \approx 12$ kpc. Virtually all of those H II regions

TABLE 2

THE z DISTRIBUTION OF H II REGIONS

R (kpc)	$\langle z \rangle$ (pc)	σ_z (pc)	n
7	5.1 ± 23.5	74.3	9
8	−25.2 ± 31.8	110.1	12
9	19.5 ± 41.0	129.5	10
10	18.2 ± 15.5	101.5	43
11	−22.0 ± 12.9	78.6	37
12	2.5 ± 9.8	57.4	34
13	55.9 ± 35.4	146.0	17
14	94.0 ± 55.8	223.0	16
>14.5	−16.8 ± 78.3	341.4	19
>14.5[a]	−36.5 ± 69.6	287.0	17

[a] If galactic plane is defined locally by the mean H I plane.

are in the Perseus arm. Because of the large number of H II regions used in calculating the dispersion in z there, the decrease is statistically significant and is an indication that the vertical scale height of H II regions and molecular clouds shows a relative decrease in spiral arms. A similar decrease is also seen at 7 kpc for H II regions associated with the Sagittarius arm, but the number of objects is small and the uncertainty in the z dispersion is relatively large. Stark (1983) has found that the most massive molecular clouds in a portion of the inner Galaxy he surveyed in ^{13}CO have a smaller scale height than the mean molecular scale height. He has identified the most massive clouds with inner Galaxy spiral arms (Stark 1979) which provides further evidence that the scale height of molecular clouds and H II regions decreases in the spiral arms of the Milky Way.

c) *The Size Distribution of* H II *Regions*

Figure 5 shows a plot of the linear diameters of the H II regions as a function of R. With only two exceptions, the maximum diameter shows an approximately exponential gradient with R: H II regions are, on average, smaller at large R. The lower envelope of this plot is likely to be due to a selection effect related to distance: very small H II regions are more difficult to detect at larger distances.

Because there are fewer H II regions in the bins at $R > 13$ kpc, we investigate whether the apparent decrease in size with radius is a statistical effect. We determine the fraction (f) of H II regions in each radial bin with sizes larger than 20 pc. The results are shown in Table 3. Column (1) is the radial bin; column (2), the number of objects in each bin; column (3) gives the number of objects with $d > 20$ pc; and column (4) gives f. For $7 < R < 12$ kpc, $f = 0.31$ and for $R > 12$ kpc, $f = 0.13$. Since f is not affected by the smaller number of objects for $R > 12$ kpc, the size decrease does appear to be significant.

Another way of looking at the statistics is to plot the third, fifth, and seventh largest H II region in each 1 kpc bin in R as shown in Figure 6. Beyond $R = 14.5$ kpc the bin size is 3 kpc. This statistic should be relatively unaffected by the selection effects because one would expect always to be able to see the largest H II regions in any radial bin. There is a sharp decrease in the number of large H II regions beyond $R = 12$ kpc which does not seem to be accounted for by the statistics. In addition H II regions in the Perseus and Sagittarius arms are apparently larger than those in the interarm region at $R = 9$ kpc, and the diameter of H II regions is smaller at even larger R. Extinction could cause the more distant H II regions to appear smaller. If there is a density gradient within an H II region, increasing line-of-sight extinction could absorb the lower emission measure extremities more effectively at larger distances. If that were the case: (1) A similar effect should

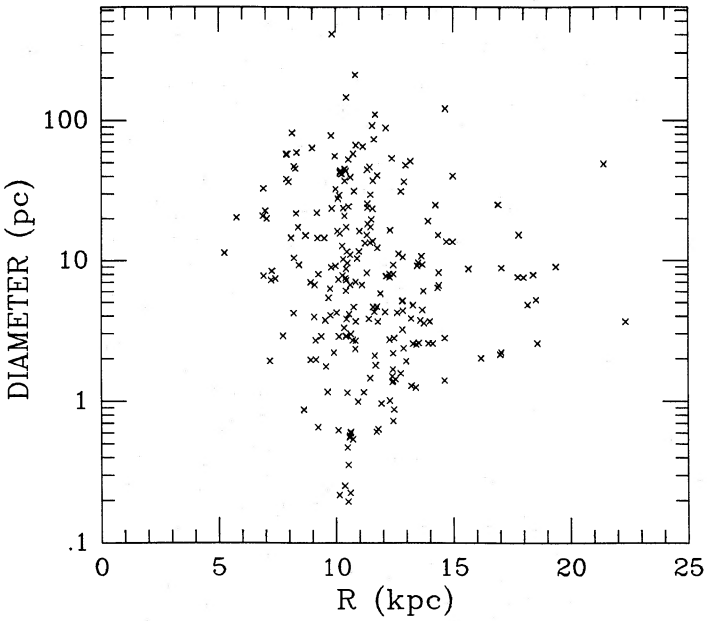

FIG. 5.—The diameter of H II regions vs. R (galactocentric distance)

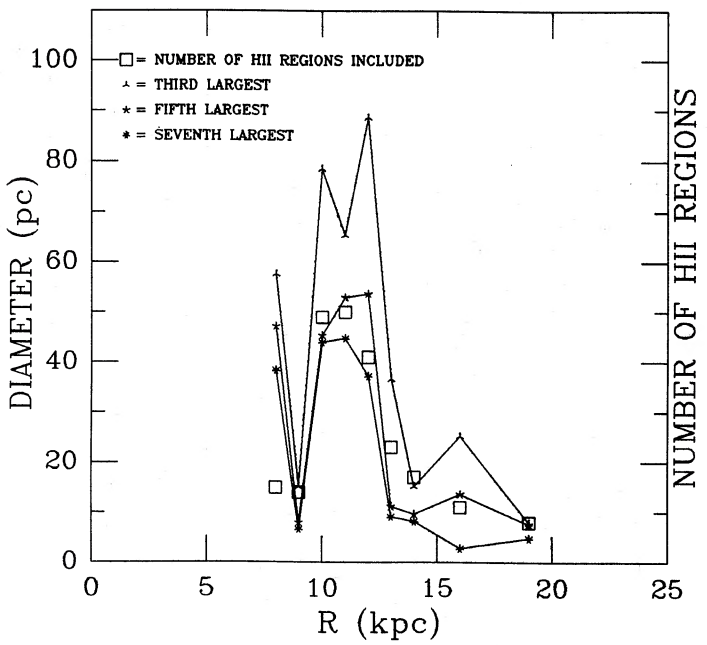

FIG. 6.—The diameter of the third, fifth, and seventh largest H II regions in 1 kpc bins in R. Beyond $R = 14.5$ kpc, the bin size is 3 kpc. The number of H II regions in each bin is shown by an open square.

occur in the inner Galaxy; Table 3 shows that it does not. (2) H II regions as bright as those seen at $R < 12$ kpc should be apparent on the radio surveys. There are however, few H II regions at 21 cm as radio bright as those seen at $R < 12$ kpc. (3) Optical extinction appears to level off at 2–3 mag for $R > 12$ kpc (see § IV*a*). Thus increasingly large extinction does not appear to be the cause of the apparent slope of the upper envelope in Figure 5.

TABLE 3

FRACTION OF H II REGIONS WITH DIAMETER > 20 PARSECS

R (kpc) (1)	N (2)	$N(D > 20$ pc) (3)	f (4)
6.5	5	4	0.8
7.5	10	5	0.5
8.5	15	6	0.4
9.5	23	5	0.22
10.5	66	19	0.29
11.5	36	12	0.33
12.5	35	5	0.14
13.5	19	1	0.05
14.5	13	3	0.23
15.5	1	0	0
16.5	2	1	0.5
17.5	4	0	0
18.5	5	0	0
19.5	1	0	0
20.5	0	0	...
21.5	1	1	1
22.5	1	0	0
AVERAGES FOR INNER AND OUTER GALAXY			
7–12	150	47	0.31
12–23	82	11	0.13

The size gradient therefore appears to be a physical property of galactic H II regions in the outer Galaxy. The gradient could be a reflection of either the stellar birthrate function at high mass or a density effect due to decreasing mean gas density beyond the solar circle.

To measure the birthrate function of the stars exciting the H II regions requires knowledge of the emission measure of the H II regions, which is related to the number of Lyman-continuum photons produced by all of the stars. This data is, however, not available at present.

H II regions expanding into a medium with a lower mean density than the local value could produce emission measures in their outer regions below the limit necessary to detect them optically, especially with a few magnitudes of intervening extinction. However, the Strömgren radius $r_s \propto n^{-2/3}$ and the emission measure $\propto n_e{}^2 r_s$; thus, the emission measure $\propto n_e{}^{4/3}$. The steepness of the decline in the sizes of H II regions beyond $R = 12$ kpc seems to indicate that this effect alone does not explain the paucity of H II regions with diameters greater than 20 pc at large R. Our data therefore appear to be weak evidence for a decrease in the efficiency with which the most massive stars form at large R.

V. CONCLUSIONS

1. H II regions are observed in the Milky Way to distances as large as $R = 20$ kpc, but there are very few beyond this distance. This limiting distance does not appear to be the result of extinction and appears to be the approximate edge of the stellar disk of the Milky Way.

2. The scale height of H II regions at $R = 10$ kpc as measured by the dispersion of z distances is ~ 100 pc, but there is considerable variation in this quantity. The smallest scale heights appear to be related to the major spiral arms.

3. Beyond $R = 12$ kpc the H II regions (and their associated

molecular clouds) follow the warp of the H I plane. Like the H I, the scale height of H II region/molecular cloud complexes increases steadily with radius.

4. H II regions are smaller, on average, at large R, and few very large H II regions are observed beyond $R = 12$ kpc. This effect may be due to either a decrease in the mean density of the ambient interstellar gas, a decrease in the efficiency with which stars of the highest mass are formed, or both.

REFERENCES

Becker, W., and Fenkert, R. B. 1970, in *IAU Symposium 38, The Spiral Structure of our Galaxy*, ed. W. Becker and G. Contopoulos (Dordrecht: Reidel), p. 205.
Blitz, L. 1978, Ph.D. thesis, Columbia University.
Blitz, L., and Fich, M. 1983, in *Kinematics, Dynamics, and Structure of the Milky Way*, ed. W. L. H. Shuter (Dordrecht: Reidel), p. 143.
Blitz, L., Fich, M., and Kulkarni, S. 1983, *Science*, **220**, 1233.
Blitz, L., Fich, M., and Stark, A. A. 1980, in *IAU Symposium 87, Interstellar Molecules*, ed. B. H. Andrew (Dordrecht: Reidel), p. 213.
———. 1982, *Ap. J. Suppl.*, **49**, 183 (BFS).
Burton, W. B., and Gordon, M. A. 1978, *Astr. Ap.*, **63**, 7.
Fich, M. 1983, Ph.D. thesis, University of California, Berkeley.
Fich, M., Treffers, R. R., and Blitz, L. 1982, in *Regioq Recent Star Formation*, ed. R. S. Rogers and P. E. Dewdney (Dordrecht: Reidel), p. 201.
Georgelin, Y. M., Georgelin, Y. P., and Sivan, J.-P. 1979, in *IAU Symposium 84, The Large Scale Characteristics of the Galaxy*, ed. W. B. Burton (Dordrecht: Reidel), p. 65.
Israel, F. P. 1979, *Astr. Ap.*, **70**, 769.
Kulkarni, S., Blitz, L., and Heiles, C. 1982, *Ap. J. (Letters)*, **259**, L63.
Kumar, C. K. 1979, *Ap. J.*, **230**, 386.
Lockman, F. J. 1979, *Ap. J.*, **232**, 761.
Mezger, P. G. 1970, in *IAU Symposium 38, The Spiral Structure of our Galaxy*, ed. W. Becker and G. Contopoulos (Dordrecht: Reidel), p. 107.
Moffat, A. F. G., FitzGerald, M. P., and Jackson, P. D. 1979, *Astr. Ap. Suppl.*, **38**, 197.
Sharpless, S. 1959, *Ap. J. Suppl.*, **4**, 257.
Stark, A. A. 1979, Ph.D. thesis, Princeton University.
———. 1983, in *Kinematics, Dynamics, and Structure of the Milky Way*, ed. W. L. H. Shuter (Dordrecht: Reidel), p. 127.

LEO BLITZ: Astronomy Program, University of Maryland, College Park, MD 20742

MICHEL FICH: Astronomy Department, FM-20, University of Washington, Seattle, WA 98195